V International Conference on Computational Methods in Marine Engineering
MARINE 2013
B. Brinkmann and P. Wriggers (Eds)

UNSTEADY FSI SIMULATION OF DOWNWIND SAILS

NICOLA PAROLINI* AND MATTEO LOMBARDI†

*MOX - Dipartimento di Matematica
Politecnico di Milano
P.zza Leonardo da Vinci, 32, 20133 Milano, Italy
e-mail: nicola.parolini@polimi.it, web page: http://mox.polimi.it

†CMCS - Mathematics Institute of Computational Science and Engineering
Ecole Polytechnique Fédérale de Lausanne
Av. Piccard, Station 8, CH-1015 Lausanne, Switzerland
e-mail: matteo.lombardi@epfl.ch, web page: http://cmcs.epfl.ch

Key words: Sail dynamics, Fluid-Structure Interaction

Abstract. A numerical model for the simulation of the fluid-structure interaction (FSI) between the wind and the sails of a sailing boat is presented. This problem is characterized by an extremely light structure (in particular when downwind sails, spinnaker or gennaker, are considered) experiencing large displacements under the action of a complex (turbulent and separated) flow field. The model is based on a strongly coupled segregated FSI approach which guarantees adequate stability properties for the FSI problem at hand. A Dirichlet-Neumann coupling algorithm is adopted with a finite-volume Reynolds Averaged Navier-Stokes (RANS) flow solver interacting with a finite-element shell structural solver. Numerical results of unsteady FSI simulations are presented and discussed.

1 INTRODUCTION

Fluid-structure interaction (FSI) problems are still subject of intensive investigation in several application fields and many different formulations have been considered in the literature for their numerical solution.

In this work, we focus on a specific application where the interaction between a fluid flow (the wind) with a flexible (and light) structure (a sail) is considered. When upwind sailing configurations are considered, the flow around the sails is mainly attached and simplified flow models based on potential flow theory can usually be adopted, as in [1, 2]. Downwind configurations are much more demanding in terms of model complexity since, on one hand, the flow around gennaker (or spinnaker) is usually detached thus requiring the solution of the full Navier–Stokes equations [3, 4, 5, 6]; on the other hand, downwind

sails can often undergo large displacements, which should be accounted for by both the structural model and the mesh motion solver.

This paper is organized as follows: in Section 2 we briefly recall the structural and fluid models adopted and we introduce an unsteady strongly-coupled FSI scheme used for wind/sail interaction problems; in Section 3, we present a numerical (space and time) convergence analysis carried on for a benchmark FSI test case and then we present the results of the FSI simulation for an unsteady downwind two-sail configuration; finally, some conclusions are drawn in Section 4.

2 FLUID-STRUCTURE INTERACTION PROBLEM

Sails are flexible structures that deform under the action of the wind. The pressure field acting on the sail changes its geometry and this, in turn, alters the flow field.

The structural and fluid solvers are briefly introduced in the following sections before describing the coupling scheme that has been devised to simulate the FSI problem as well as the numerical techniques adopted for the interface data transfer and for the mesh motion. A detailed description of the different components of the FSI solver can be found in [7].

2.1 Structural solver

To model the structural behavior of the sails subjected to an external stress field we consider a shell finite element approach. Given a shell body of constant thickness h immersed in a fixed reference frame $\{\mathbf{e}_i\}$, $i = 1, 2, 3$ and based on the inextensible director shell theory, the geometry of the shell in the reference configuration is given by the mapping

$$\mathbf{X} = \mathbf{\Phi}(\bar{\boldsymbol{\xi}}) = \bar{\mathbf{\Phi}}(\xi^1, \xi^2) + \xi^3 \mathbf{L}(\xi^1, \xi^2), \qquad -\frac{h}{2} \leq \xi^3 \leq \frac{h}{2}, \tag{1}$$

where $\mathbf{X}$ is the position vector of a material point in the shell body identified by the convective system of coordinates $\bar{\boldsymbol{\xi}} = (\xi^1, \xi^2, \xi^3)$; $\bar{\boldsymbol{X}} = \bar{\mathbf{\Phi}}(\xi^1, \xi^2)$ are the points on the shell middle surface $\mathcal{M}(\xi^3 = 0)$, with boundary $\partial\mathcal{M}$, and the unit vector $\mathbf{L}(\xi^1, \xi^2)$ denotes the director field. We assume $\mathbf{L}$ to be normal to the middle surface in the original configuration but this property s, in general, lost during the deformation. Moreover, we assume that the material line originally normal to the shell midsurface in the reference configuration remains straight and unstretched during motion and that the stresses in the direction of the material line are zero.

A shell deformed configuration at time $t \in [0, T]$ is defined by the mapping $\mathbf{x} = \chi_t(\mathbf{X})$ where χ_t represents the motion. For this kinematics, the displacements $\mathbf{d}$ at a generic point $\mathbf{X}$ is given by

$$\mathbf{d}(\bar{\boldsymbol{\xi}}) = \mathbf{x}(\bar{\boldsymbol{\xi}}) - \mathbf{X}(\bar{\boldsymbol{\xi}}). \tag{2}$$

For a solid with density ρ_0 subjected to forces $\mathbf{B}$, the equation of motion (balance of momentum) in the reference configuration reads:

$$\rho_0 \frac{\partial^2 \mathbf{d}}{\partial t^2} = \nabla_R \cdot \mathbf{S} + \mathbf{B}, \tag{3}$$

where $\nabla_R \cdot$ is the divergence operator in the reference configuration and $\mathbf{S} = J\boldsymbol{\sigma}_S \mathbf{F}^{-T}$ is the first Piola-Kirchhoff stress tensor, $\boldsymbol{\sigma}_S$ is the Cauchy stress tensor, $\mathbf{F}$ is the deformation gradient defined as

$$\mathbf{F} = \frac{\partial \chi_t(\mathbf{X}, t)}{\partial \mathbf{X}} = \frac{\partial \mathbf{x}(\mathbf{X}, t)}{\partial \mathbf{X}},$$

and J is the determinant of $\mathbf{F}$.

The spatial discretization of problem (3) is based on the finite element method using the MITC4 elements [8]. This approach proved to be adequate [9] to simulate the dynamics of light structures, in particular with respect to the typical occurrence of post-buckled configurations triggered by local instabilities, known as *wrinkling*. A time adaptive explicit second-order scheme is considered for the time discretization (see [7]).

2.2 Fluid solver

In the context of sails simulations, potential flow models have been used extensively in case of upwind sailing configurations where the flow can be considered mainly attached. For downwind configurations, large flow separations usually occur and thus the solution of the full Navier-Stokes equations is required. Due to the typical Reynolds number characterizing the problem, a turbulence model approach is required and the Reynolds Averaged Navier-Stokes (RANS) equations are considered, which read

$$\begin{cases} \dfrac{\partial(\rho\mathbf{u})}{\partial t} + \boldsymbol{\nabla} \cdot (\rho\mathbf{u} \otimes \mathbf{u}) - \boldsymbol{\nabla} \cdot \boldsymbol{\sigma}_F = \mathbf{0}, & \text{in} \quad \Omega(t) \times (0,T), \\ \boldsymbol{\nabla} \cdot \mathbf{u} = 0 & \text{in} \quad \Omega(t) \times (0,T), \\ \mathbf{u} = \mathbf{u}_0 & \text{in} \quad \Omega(t=0), \\ \mathbf{u} = \mathbf{u}_D & \text{on} \quad \Gamma_D \times (0,T), \\ \boldsymbol{\sigma}_F \cdot \mathbf{n} = \mathbf{0} & \text{on} \quad \Gamma_N \times (0,T), \\ \mathbf{u} = \dot{\mathbf{d}} & \text{on} \quad \Gamma_{Sail}(t) \times (0,T) \end{cases} \tag{4}$$

where $\mathbf{u}$ and p are the averaged velocity and pressure, ρ is the air density, $\mathbf{w}$ is the mesh velocity and $\boldsymbol{\sigma}_w = \mu(\boldsymbol{\nabla}\mathbf{u} + \boldsymbol{\nabla}\mathbf{u}^T) - p\mathbf{I}$ is the stress tensor, with $\mu_{\text{eff}} = \mu + \mu_t$ denoting the total viscosity (sum of the dynamic and turbulent viscosity). On the portion Γ_D of the domain boundary (which usually includes the inlet), a Dirichlet velocity boundary condition $\mathbf{u}_D$ is imposed while on Γ_N (usually the outlet boundary) a Neumann-type condition imposes zero normal stress. The velocity on the moving sail is equal to $\dot{\mathbf{d}}$, the rate of deformation of the structure interpolated on the fluid interface. The turbulent

viscosity is evaluated using the Shear-Stress-Transport (SST) model [10] which requires the solution of two additional partial differential equations for the turbulent kinetic energy ε and for the specific dissipation ω, which are solved in a segregated fashion with respect to problem (4). Note that, in order to deal with the moving domain due to the sail deformation, a Arbitrary Lagrangian Eulerian (ALE) formulation of the RANS equations [11] has been adopted.

2.3 Mesh motion

The third computational ingredient of the FSI algorithm has to deal with the fluid mesh motion. Indeed, on one hand, the structural solver is based on a Lagrangian approach in which the problem is always recasted into a reference structural domain; on the other hand, the ALE approach adopted in the flow solution requires the extension of the sail displacement to the whole fluid domain. Different approaches can be adopted to face this problem. In this work, we have considered a technique based on the Inverse Distance Weighting (IDW) interpolation [12].

2.4 FSI coupling

Let us denote with $\mathcal{F}$ the fluid problem (4) defined on domain $\Omega_F(t)$ and with $\mathcal{S}$ the structural problem (3) defined on domain $\Omega_S(t)$. Moreover, we denote with $\mathcal{M}$ the mesh motion problem that is solved at each iteration to adapt the fluid computational grid to the updated sail geometry. In mathematical terms, the FSI problem can be defined as a coupled system that comprises the fluid problem $\mathcal{F}$, the structural problem $\mathcal{S}$ and the mesh motion problem $\mathcal{M}$. In abstract form, the problem can be formulated as follows

$$\begin{cases} \mathcal{F}(\mathbf{u}, p, \mathbf{w}) = 0 & \text{in} \quad \Omega_F(t) \\ \mathcal{S}(\mathbf{d}) = 0 & \text{in} \quad \Omega_S(t) \\ \mathcal{M}(\boldsymbol{\eta}) = 0 & \text{in} \quad \Omega_F^0 \\ & \\ \mathbf{u} = \dot{\mathbf{d}} & \text{on} \quad \Gamma(t) \\ \boldsymbol{\sigma}_F(\mathbf{u}, p)\mathbf{n}_F = \boldsymbol{\sigma}_S(\mathbf{d})\mathbf{n}_S & \text{on} \quad \Gamma(t) \\ \boldsymbol{\eta} = \mathbf{d} & \text{on} \quad \Gamma^0 \,, \end{cases} \tag{5}$$

where the three (fluid, structure and mesh motion) problems are coupled through three conditions over the interface $\Gamma(t)$ stating the continuity of velocity, the equilibrium of forces and the geometric continuity, respectively. In (5), $\boldsymbol{d}$ denoted the structural displacement, $\boldsymbol{\eta}$ the mesh displacement, Ω_F^0 and Γ^0 denote the reference fluid domain and interface, respectively. The fluid mesh motion velocity $\mathbf{w}$, needed in the ALE formulation of the RANS equations, is the time-derivative of the mesh displacement $\mathbf{w} = \dot{\boldsymbol{\eta}}$.

For the solution of problem (5), different FSI schemes can be devised. *Monolithic* schemes are based on the solution of a global system which is assembled and solved for

all the unknowns of the problem simultaneously; on the other hand, when existing (and independent) fluid and structural solvers have to be coupled, *partitioned* schemes, in which the fluid, structure and mesh motion problems are solved iteratively, are preferred. For the case at hand, a strongly-coupled partitioned scheme has been devised, which guarantees that at each time step the equilibrium is reached between the different sub-problems. To compute the solution at time t^{n+1}, a sub-iteration between the three sub-problems is required. The structural solution is first computed

$$\begin{array}{ll} \mathcal{S}(\mathbf{d}_{k+1}^{n+1}) = 0 & \text{in } \Omega_{S_k}^{n+1} \\ \boldsymbol{\sigma}_S(\mathbf{d})_{k+1}^{n+1}\mathbf{n}_{S_k}^{n+1} = \boldsymbol{\sigma}_F(\mathbf{u},p)_k^{n+1}\mathbf{n}_{F_k}^{n+1} & \text{on } \Gamma, \end{array}$$

followed by the mesh motion update

$$\begin{array}{ll} \mathcal{M}(\boldsymbol{\eta}_{k+1}^{n+1}) = 0 & \text{in } \Omega_F^0 \\ \boldsymbol{\eta}_{k+1}^{n+1} = \alpha\mathbf{d}_{k+1}^{n+1} + (1-\alpha)\mathbf{d}_k^{n+1} & \text{on } \Gamma^0, \end{array}$$

and finally the flow solution

$$\begin{array}{ll} \mathcal{F}(\mathbf{u}_{k+1}^{n+1}, p_{k+1}^{n+1}, \mathbf{w}_{k+1}^{n+1}) = 0 & \text{in } \Omega_{F_{k+1}}^{n+1} \\ \mathbf{u}_{k+1}^{n+1} = \alpha\dot{\mathbf{d}}_{k+1}^{n+1} + (1-\alpha)\dot{\mathbf{d}}_k^{n+1} & \text{on } \Gamma_{k+1}^{n+1}, \end{array}$$

where α is a coefficient computed using the Aitken relaxation. The iteration over the index k is stopped when a suitable convergence criterion is fulfilled, namely

$$\begin{cases} ||\mathbf{d}_{k+1}^{n+1} - \mathbf{d}_k^{n+1}||/||\mathbf{d}_0^{n+1}|| \leq \epsilon_d \\ ||\mathbf{u}_{k+1}^{n+1} - \mathbf{u}_k^{n+1}||/||\mathbf{u}_0^{n+1}|| \leq \epsilon_u \\ ||p_{k+1}^{n+1} - p_k^{n+1}||/||p_0^{n+1}|| \leq \epsilon_p \end{cases},$$

where both L^2 and L^∞ norms have been tested. In the numerical tests discussed in Section 3, a convergence criterion based on the L^2 norm has been used.

The FSI scheme described above can be adopted when non-conforming (at the interface) space discretizations are adopted for the fluid and structural problems. In this case, suitable interpolation operators for the data transfer at the interface are required. The approach adopted in this work is based on Radial Basis Functions and was introduced in [13]. Non-conforming interface grids are considered, for example, in the FSI sail simulation that will be presented in Section 3.2.

3 NUMERICAL RESULTS

The strongly-coupled FSI algorithm introduced in the previous sections has been applied for the simulation of different sail configurations. For an overview of the results, we refer to [7], where a large set of simulations on one- and two-sail configurations are discussed, together with an analysis of the effect of the sail trimming.

In order to assess the convergence properties of the model, we present here a simple benchmark test case comparing our results with those published in the literature. Moreover, to display the ability of the model in capturing complex sail dynamics, we report the result of an unsteady numerical simulation on a two-sail downwind configuration.

3.1 Cavity with flexible wall

As in the test case proposed in [14], a three-dimensional cavity with flexible bottom is considered with a pulsating flow field imposed on a small inlet section on the upper part of one side, while, on the opposite side a small outlet section is present.

On the inlet section, a pulsating linear velocity profile in $x-$direction, ranging from $\mathbf{0}$ to

$$\mathbf{u}_{\text{top}}(t) = (1 - \cos(2\pi t/5), 0, 0),$$

with a period of 5 s is considered. On the top surface, a uniform Dirichlet boundary condition $\mathbf{u} = \mathbf{u}_{\text{top}}$ is imposed, while on the outlet boundary the normal stress is set to zero. The flexible bottom surface is modeled using the shell finite element model described in Section 2.1 and the FSI interface conditions introduced in Section 2.4 apply. Finally, on the remaining boundaries homogeneous Dirichlet boundary conditions $\mathbf{u} = \mathbf{0}$ are imposed. The fluid and structural physical properties are reported in Table 1.

Fluid	Density [Kg/m^3]	Viscosity [m^2/s]	Cavity size [m]	Inlet size [m]
	1.0	0.01	1	0.125
Structure	Density [kg/m^3]	Poisson's ratio	Young's modulus [N/m^2]	Thickness [m]
	500	0.0	250.0	0.002

Table 1: Fluid and structural properties used in the cavity test case.

In Figure 1, the deformation undergone by the flexible bottom and the streamlines on the longitudinal vertical midplane are reported for different time instants. The pulsating flow field generates a suction pressure on the bottom and the creation of a large vortex inside the fluid domain.

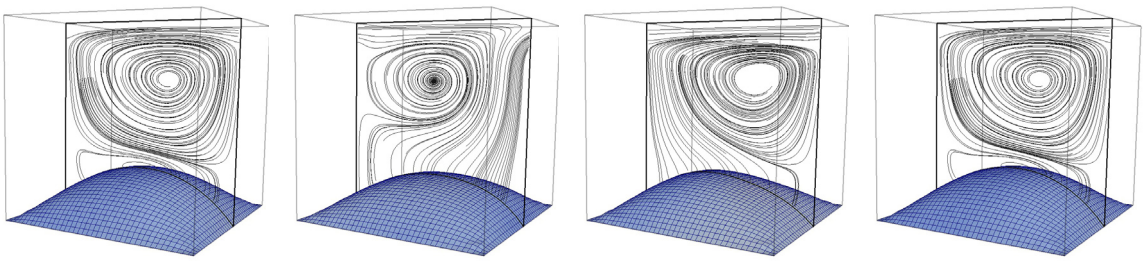

Figure 1: Structural surface deformation and fluid streamlines on a vertical cross section at different time instant over a period.

The time evolutions of the vertical displacement of the bottom surface midpoint are displayed in Figure 2 for different resolutions and show the space and time convergence of the method. The results are in agreement with those obtained in [14] where, however, no convergence analysis is reported.

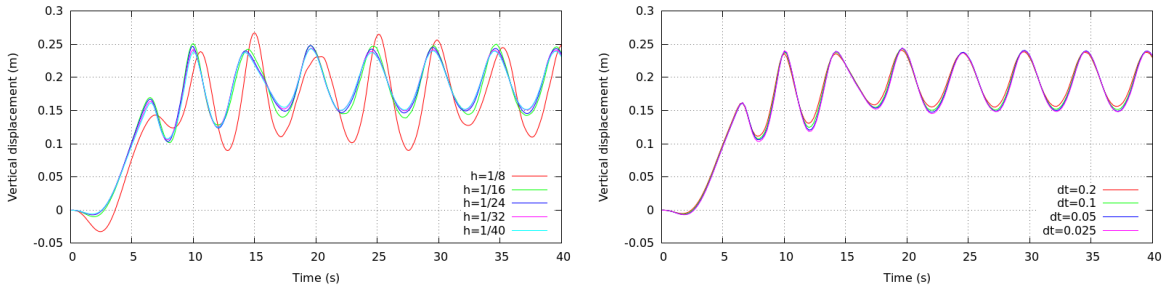

Figure 2: Time evolution of the bottom surface midpoint displacement: space (left) and time (right) convergence.

3.2 Unsteady FSI simulation for downwind sails

In this section, we present the results of the unsteady FSI simulation of a two-sail configuration. Only the sails are considered in this simulation and the computational domain is a parallelepiped surrounding them. The computational grid is based on a hybrid approach, where in the far field region a block structured grid is generated, while in a small region around the sails an unstructured grid is used (see Figure 3). The gennaker has two fixed vertices and the third one, attached to the trimming sheet, as the sheet is in tension, is constrained to stay at a fixed distance from the attachment point on the boat, thus moving on a spherical surface. The main sail motion is much more constrained, as the side attached to the mast is fixed (no mast deformation is considered), as well as the side attached to the boom.

The velocity boundary conditions imposed at the inlet of the domain is the composition of the opposite of the boat speed (here equal to 5.48 m/s in the $x-$direction) and the wind velocity (see Figure 4, left). The wind velocity magnitude is modeled with the following

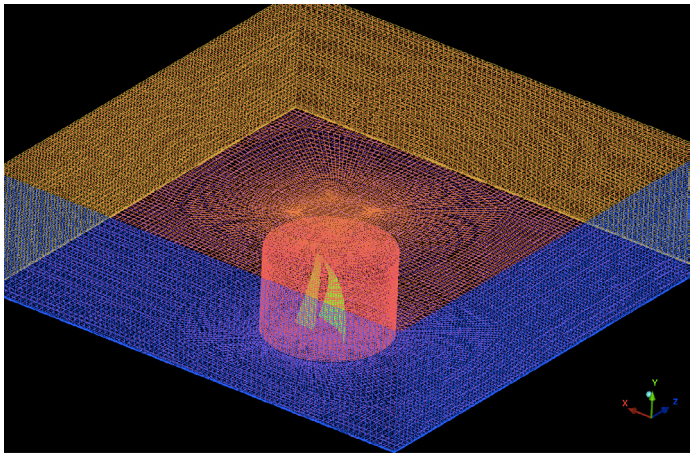

Figure 3: Hybrid structured-unstructured mesh for the gennaker-main sail simulations. The cylinder surface delimits the unstructured domain.

atmospheric boundary layer law (assuming y the vertical axis pointing upwards and the sea level being at y =0 m):

$$u(y) = u_{ref} \left(\frac{y}{y_{ref}} \right)^{C_r} \tag{6}$$

where u_{ref} is the reference wind velocity at the reference height y_{ref} and C_r is a constant reflecting the roughness of the surface over which the wind is blowing. In our simulations, we considered the reference wind velocity $u_{ref} = 6.632$ m/s, the reference height $z_{ref} = 10$ m and the roughness constant $C_r = 0.1$. In the downwind configurations considered here the boat is *reaching*: the wind is coming diagonally from behind, with an angle equal to 155 degrees to the bow direction.

These choices result in a twisted profile imposed on the inflow boundary: the resulting velocity profile is in fact the opposite of the boat speed at sea level but rapidly change direction and magnitude as the height increases (see Figure 4, right).

In order to be able to simulate such flow boundary layer accurately and preserve it inside the fluid domain, a refinement in the vertical direction of the computational grid in the area close to the sea level is required.

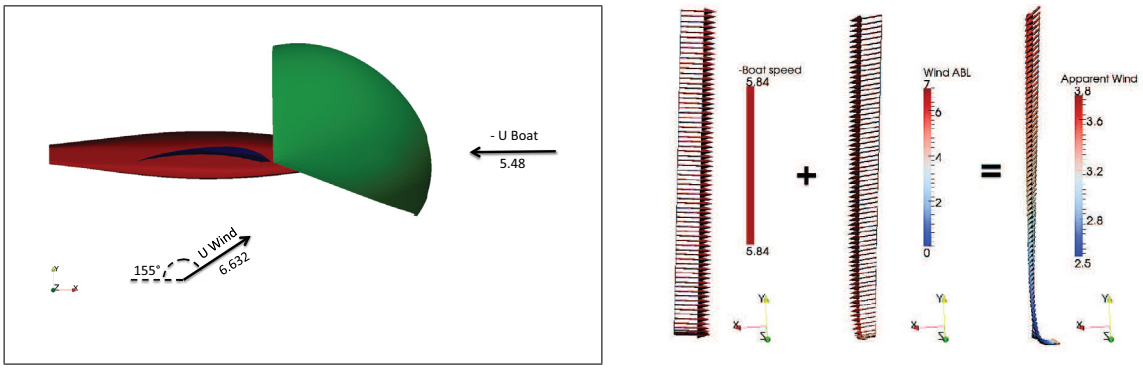

Figure 4: Boat velocity and wind speed directions (left) and resulting twisted inflow boundary condition (right).

The sail fabric is modeled with a simple isotropic constitutive law, while the presence of battens (stiff elements inserted in the main sail to better control its shape) is accounted for considering local changes in the structure mechanical properties. The fluid and structural physical properties are reported in Table 2.

The deformation undergone by the sails can be observed in Figures 5 and 6. In the first instants, the vertex attached to the trimming sheet is free to move and travel forward under the pressure of the wind being the sheet not yet under tension (Figures 5, (a)). Being the bow vertex fixed, a wrinkle is generated in the lower forward part of the sail. When the maximum sheet length is reached, the motion of the sheet attached vertex is abruptly stopped and the sheet starts pulling down and backward: such impulse propagates very quickly from the vertex upward (Figure 5, (b)-(c)-(d)) and merges with the

one propagating from the bow wrinkle. After 2.8 seconds the deformation is already quite small and the simulation very close to a steady solution.

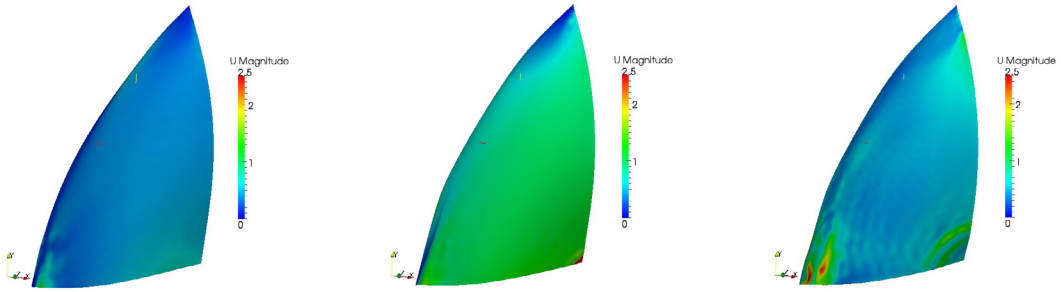

(a) Time = 0.5 $[s]$. (b) Time = 1.0 $[s]$. (c) Time = 1.2 $[s]$.

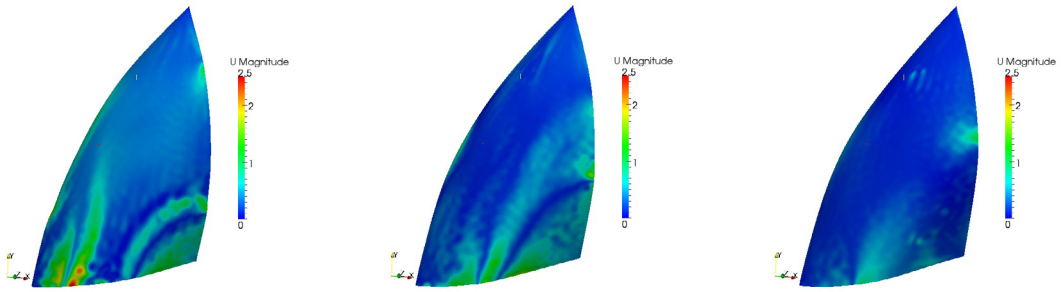

(d) Time = 1.5 $[s]$. (e) Time = 2.0 $[s]$. (f) Time = 2.8 $[s]$.

Figure 5: Two-sail transient FSI simulation: gennaker time evolution colored by displacement velocity contour.

The motion undergone by the main sail is much smaller if compared with the one of the gennaker due to the higher stiffness of the sail and, more importantly, to the very constraining boundary conditions. It is interesting to notice though that the presence of the battens, modeled with a local higher Young's modulus, has an influence on the motion, as can be observed in Figure 6, (a). The displacement of the main sail is characterized by deformation waves almost aligned with the vertical axis and propagating from the mast to the rear of the sail: once again this is physically compatible with the imposed constraints over the sail edges.

Fluid	Density $[Kg/m^3]$	Viscosity $[m^2/s]$		
Air	1.0	$1.5\ 10^{-5}$		
Structure	Density $[kg/m^3]$	Poisson's ratio	Young's modulus $[N/m^2]$	Thickness $[m]$
Gennaker	100	0.3	$3.76\ 10^{8}$	0.001
Main sail	340	0.3	$1.93\ 10^{9}$	0.003
Battens	500	0.3	$1.0\ 10^{10}$	0.012

Table 2: Fluid and structural properties used in the wind/sails FSI simulations.

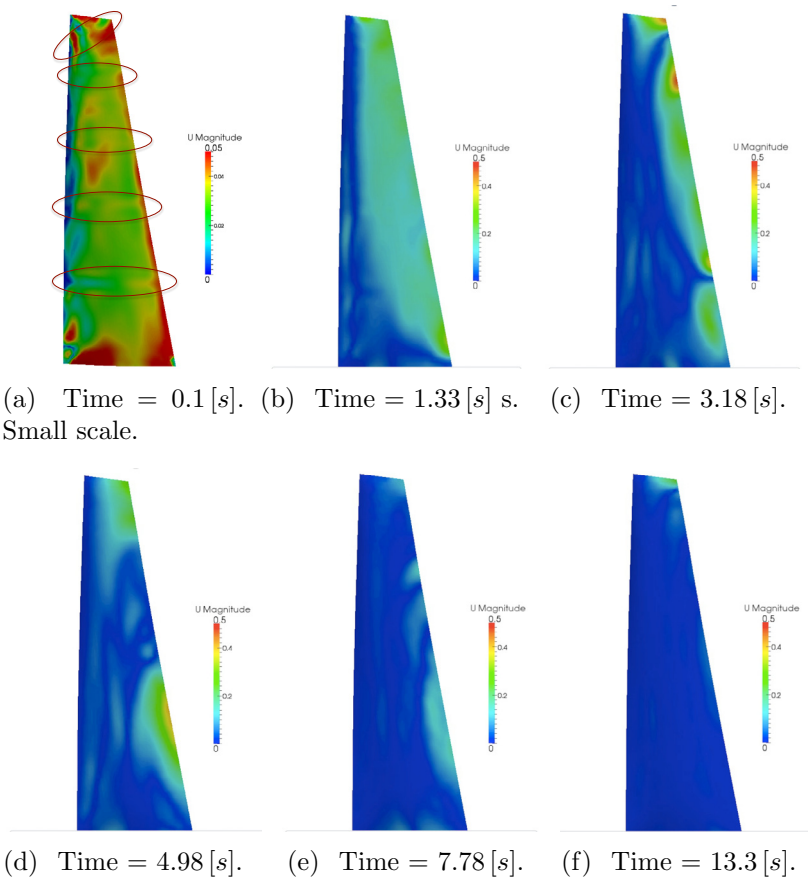

(a) Time = 0.1 [s]. (b) Time = 1.33 [s] s. (c) Time = 3.18 [s]. Small scale.

(d) Time = 4.98 [s]. (e) Time = 7.78 [s]. (f) Time = 13.3 [s].

Figure 6: Two-sail transient FSI simulation: main sail time evolution colored by displacement velocity contour.

The time evolution of the forward force on the gennaker is displayed in Figure 7. In the first instants, the forward force on the gennaker drops to a very low value while the gennaker trimming sheet is not yet under tension and the sail is free to open up. When the trimming sheet starts pulling, the force abruptly rises to a large value and only slowly stabilize to an asymptotic regime when the sail is almost at rest. Nonetheless, a small fluctuation can still be observed even at convergence, showing that the asymptotic solution is unsteady and thus justifying the adoption of an unsteady FSI solver. In Figure 7, the present unsteady result is compared to the converged force value on the initial geometry configuration and to that obtained by a steady FSI simulation, where steady versions of both flow and structural solvers are considered.

Regarding the computational cost of such simulation, it is worth mentioning that, given a fixed FSI coupling tolerance, the residuals over the main sail converge much faster than those over the gennaker sail, due to much smaller motion magnitude. The structural solvers for the two sails are run independently, with the one simulating the main sail takes the longest time for each structural solution (being the sail stiffer, a smaller time step

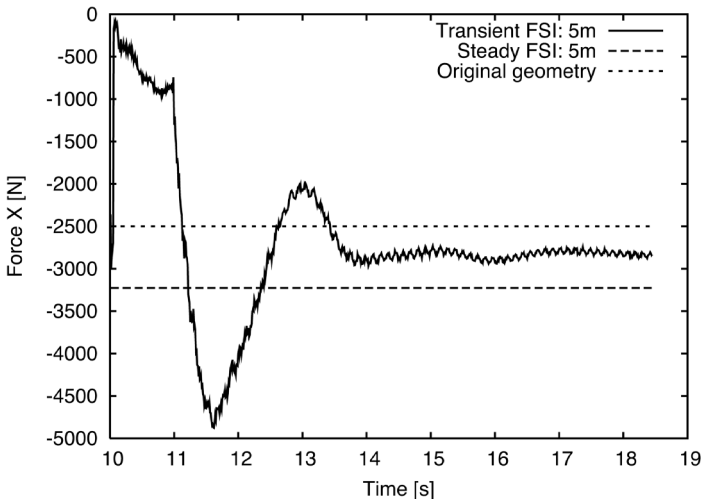

Figure 7: Two-sail transient FSI simulation: time evolution of the forward force on the gennaker.

constraint is imposed to the explicit solver to be able to catch the higher frequencies).

4 CONCLUSIONS

A model for the simulation of the unsteady dynamics of sails interacting with the wind has been presented. The model has been conceived in order to guarantee the strict stability requirements needed by fluid-structure interaction problems with light structure. In this respect, a strongly-coupled partitioned approach was considered with a FSI sub-iteration reaching a dynamic equilibrium at each time step. Moreover, an energy preserving interface data transfer between the fluid and the structure was used at the non-conforming interface. The convergence and robustness of the method have been assessed with numerical results on both an academic FSI test case and a real downwind sail dynamic problem.

REFERENCES

[1] T. Fukasawa and M. Katori. Numerical approach to aeroelastic responses of three-dimensional flexible sails. In *Proc. of 11th Chesapeake Sailing Yacht Symposium (Annapolis)*, 1993.

[2] J. Pilate. Development of a three-dimensional inverse sail design method. In *Proceedings 3rd High Performance Yacht Design Conference*, 2008.

[3] N. Parolini and A. Quarteroni. Mathematical models and numerical simulations for the America's cup. *Computer Methods in Applied Mechanics and Engineering*, 194:pp. 1001–1026, 2005.

[4] H. Renzsch, O. Müller, and K. Graf. Flexsail – a fluid structure interaction program for the investigation of spinnakers. In *Proceedings 2nd High Performance Yacht Design Conference*, 2006.

[5] D. Detomi, N. Parolini, and A. Quarteroni. Numerical models and simulations in sailing yacht design. In M. Peters, editor, *Computational Fluid Dynamics for Sport Simulation*, pages 1–31. Springer, 2009.

[6] Ignazio Maria Viola. Downwind sail aerodynamics: A cfd investigation with high grid resolution. *Ocean Engineering*, 36(1213):974 – 984, 2009.

[7] M. Lombardi. *Numerical simulation of a sailing boat: free surface, fluid structure interaction and shape optimization*. PhD thesis, EPFL, 2012.

[8] E. N. Dvorkin, D. Pantuso, and E. A. Repetto. A formulation of the MITC4 shell element for finite strain elasto-plastic analysis. *Computer Methods in Applied Mechanics and Engineering*, 125:pp. 17–40, 1995.

[9] D. Trimarchi, S. R. Turnock, D. J. Taunton, and D. Chapelle. The use of shell elements to capture sail wrinkles, and their influence on aerodynamic loads. In *The Second International Conference on Innovation in High Performance Sailing Yachts (Lorient, France)*, 2010.

[10] F. R. Menter, M. Kuntz, and R. Langtry. Ten years of industrial experience with the SST turbulence model. *Heat and mass transfer*, 4:pp. 625–632, 2003.

[11] J. Donea, S. Giuliani, and J.P. Halleux. An arbitrary Lagrangian-eulerian finite element method for transient dynamic fluid-structure interactions. *Computer Methods in Applied Mechanics and Engineering*, 33:pp. 689–723, 1982.

[12] J. Witteveen and H. Bijl. Explicit mesh deformation using inverse distance weighting interpolation. In *Proceedings of 47th AIAA Aerospace Sciences Meeting*, 2009.

[13] M. Lombardi, N. Parolini, and A. Quarteroni. Radial basis functions for inter-grid interpolation and mesh motion in fsi problems. *Computer Methods in Applied Mechanics and Engineering*, 256(0):117 – 131, 2013.

[14] J. G. V. Vázquez. *Nonlinear Analysis of Orthotropic Membrane and Shell Structures Including Fluid-Structure Interaction*. PhD thesis, Universitat Politècnica de Catalunya, 2007.